Article:
Bauman, D, Fortunel, C, Delhaye, G et al. (16 more authors) (2022) Tropical tree mortality has increased with rising atmospheric water stress. Nature, 608 (7923). pp. 528-533. ISSN 0028-0836

https://doi.org/10.1038/s41586-022-04737-7

Tropical tree mortality has increased with rising atmospheric water stress

Authors

David Bauman[1,2,3]*, Claire Fortunel[3], Guillaume Delhaye[4,2], Yadvinder Malhi[2], Lucas A. Cernusak[5], Lisa P. Bentley[6], Sami W. Rifai[7,8], Jesús Aguirre-Gutiérrez[2,9], Imma Oliveras Menor[2,3], Oliver L. Phillips[10], Brandon E. McNellis[11], Matt Bradford[12], Susan G. W. Laurance[5], Michael F. Hutchinson[13], Raymond Dempsey[5], Paul E. Santos-Andrade[14], Hugo R. Ninantay-Rivera[14], Jimmy R. Chambi Paucar[14], Sean M. McMahon[1]

Affiliations

[1] Smithsonian Environmental Research Center, Edgewater, Maryland 21037, USA.

[2] Environmental Change Institute, School of Geography and the Environment, University of Oxford, Oxford, UK.

[3] AMAP (Botanique et Modélisation de l'Architecture des Plantes et des Végétations), Université de Montpellier, CIRAD, CNRS, INRAE, IRD, Montpellier, France.

[4] Ecosystem Stewardship, Royal Botanic Gardens Kew. UK.

[5] Centre for Tropical Environmental and Sustainability Science, College of Science and Engineering, James Cook University, Cairns, Queensland 4878, Australia.

[6] Department of Biology, Sonoma State University, 1801 E. Cotati Ave., Rohnert Park, CA 94928 USA.

[7] ARC Centre of Excellence for Climate Extremes, University of New South Wales, Sydney, NSW, Australia.

[8] Department of Environmental Science, Policy, and Management, UC Berkeley, CA, USA.

[9] Biodiversity Dynamics, Naturalis Biodiversity Center, Leiden, The Netherlands.

[10] School of Geography, University of Leeds, Leeds, UK.

[11] Southwest Biological Science Center, U.S. Geological Survey. Moab, UT, USA.

[12] CSIRO Land and Water, Tropical Forest Research Centre, Atherton, Queensland, Australia.

[13] Fenner School of Environment and Society, The Australian National University, Canberra, Australia.

[14] Universidad Nacional San Antonio Abad del Cusco, Cusco, Perú.

*Corresponding author - email: david.bauman@oxfordecosystems.co.uk

Abstract

There is evidence that tree mortality is accelerating in some regions of the tropics [1,2], with profound consequences for the future of the tropical carbon sink and the global anthropogenic carbon budget left to limit peak global warming below 2 °C. However, the mechanisms that may be driving such mortality changes and whether particular species are especially vulnerable remain unclear [3–8]. We analyse a 49-year record of tree dynamics from 24 old-growth forest plots encompassing a broad climatic gradient across the Australian moist tropics and find that annual tree mortality risk has, on average, doubled across all plots and species over the last 35 years, indicating a potential halving in life expectancy and carbon residence time. Associated biomass losses were not offset by gains from growth and recruitment. Plots in less moist local climates presented higher average mortality risk, but local mean climate did not predict the pace of temporal increase in mortality risk. Species varied in the trajectories of their mortality risk, with the highest average risk found nearer the upper end of species' atmospheric vapour pressure deficit niches. A long-term increase in vapour pressure deficit was evident across the region, suggesting thresholds involving atmospheric water stress, driven by global warming, may be a primary cause of increasing tree mortality in moist tropical forests.

Tropical forests are critical to the global carbon cycle, and shifts in their long-term dynamics can influence the pace of climate change. There are indications of slowing carbon accumulation in some tropical forests primarily due to changes in mortality [1,2], but uncertainty remains in the scope, severity, and mechanisms that might result in global tropical forest structure and dynamics changes [3–8]. If the tropical forest carbon sink (estimated at 1.2 Pg C $year^{-1}$ for recent decades [9]) declines rapidly to zero, the available anthropogenic emissions "carbon budget" to stay below 1.5 °C by mid-century declines from 120 Pg C to about 100 Pg C, and to stay below 2 °C by 2100 it declines from 374 Pg C to about 320 Pg C [10,11]. Hence, the causes and future of tropical forest tree mortality have important consequences for our prospects to stabilise global climate within safe limits.

Predicting tree mortality is especially challenging given the multiple pathways through which climate can induce mortality and the ways in which different species respond to climate change. Specifically, mortality due to water limitation can result from long-term shifts in climate, specific extreme events, or their interaction [2,4,12,13]. For example, temperature could increase tree mortality directly by increasing physiological thermal stress [14,15] or indirectly by increasing atmospheric evaporative demand (i.e. vapour pressure deficit, VPD) [7,16–19], while increasing seasonality in the tropics and subtropics would increase soil water stress and decrease dry season water supply [20]. These processes increase the probability of death through a series of potential mechanisms (e.g., hydraulic failure, carbon starvation [7,12,13,21,22]). In particular, some studies suggest that tropical forests on the drier edge of the biome's range may be closer to a tolerance threshold and hence more vulnerable to water stress as revealed by reductions of growth [23], increases in mortality [24,25], and decreases in population size [26,27]. However, other work suggests that compositional diversity in forests near this dry edge might provide buffers against forest dieback, with some taxa or regions suffering less from water stress [3,6]. Improving our understanding of mortality dynamics requires quantifying mortality patterns along climatic gradients with an explicit consideration of taxon-level vulnerability to environmental constraints. As such, long-term demographic datasets along these gradients are uniquely capable of disentangling patterns in mortality from their potential mechanisms in a way that can inform predictions [28]. However, analyses of the infrequent and stochastic nature of mortality require sustained, long-term monitoring, which is rare, especially in the tropics.

Using tropical forest demographic data spanning 49 years, we analysed temporal patterns of tree mortality for 81 dominant tree species encompassing 74,135 observations of stems above 10 cm

diameter across 24 tropical moist forest plots along an elevation gradient in North Queensland, Australia (Tables S1, S2). We estimated the probability of mortality (hereafter, 'mortality risk') across stems, species, plots and years (eqs. 1 in Methods; Figs. S1, S2). Analysing the yearly distribution of mortality risk across all plots and species from 1971 through 2019 (model M1; see Methods), we show that after a period of slight mortality risk decline, the baseline risk increased, with several years standing out as high-risk years. A change-point analysis on these data confirmed a transition from moderately decreasing to increasing mortality risk occurring in the mid-1980's (the analysis indicating 1984) (model M2; Tables S3, S4). This modelled shift is also evident in the observed mortality rates across plots and census intervals (Fig. 1b). The mechanisms responsible for the increase in mortality risk are associated with secular long-term climate change (notably an increase in temperature and atmospheric water vapour pressure deficit, VPD) (Fig. 1c) and wind-disturbance events due to cyclones (black triangles in Fig. 1b).

The mortality risk estimated per stem and year from the census data were used as response variables in a series of Bayesian multilevel analyses (models M1-M6; Table S4) to test temporal patterns of mortality risk after 1984 across plots and species and investigate potential underlying mechanisms associated with those patterns. We focused on the effect of VPD and maximum daily air temperature (Tmax) to explain differences in both average mortality risk and its rates of change over time among plots, as both VPD and temperature have increased in all 24 plots in the past 49 years and have reduced tree growth (Fig. 1c; Bauman et al. [23]), and are candidates in increasing forest stress globally [2,29,30]. To capture the potential influence of soil water supply on tree water stress and rainfall seasonality, we also used maximum climatological water deficit (MCWD) as an additional predictor. Specifically, we used Tmax and VPD of the year's driest quarter, and MCWD, averaged over 35 years (1984-2019; M3, see Table S4).

We found an increase in plot-level average mortality risk between 1984 and 2019 in 21 of the 22 plots with at least three censuses (Figs. 2, 3a, Table S5; grand 'year' slope (eqs. 3): β_0 = 0.23 [0.29, 0.17], median and 95%-highest posterior density interval (HPDI)) with a five-fold difference in the rate of mortality risk change over time along the climate gradient ('among-plot' variation in 'year' slope: σ_β = 0.16 [0.12, 0.21]; Fig. 3a; see eqs. 3 in Supp. Methods S1). Model predictions indicated a doubling in average mortality risk across plots between the 1980s and 2010s (model M3; Fig. 3a), corresponding to a potential halving of tree life expectancy and carbon residence time [31]. None of the mean climate predictors explained the variation in the slope of temporal change of mortality risk among plots (Table S5, Fig. S3); drier plots were no more vulnerable to

increased mortality risk than more moist plots. The overall plot-specific average mortality risk (α_k, eqs. 3), however, was higher in warmer and drier plots (Fig. 2, Fig. S3; α_1 (VPD): 0.30 [0.49, 0.12], and α_1 (Tmax): 0.37 [0.52, 0.23]). Plot average MCWD showed no evidence of an association with mortality risk (Table S5). Cyclones occurred in a subset of plots (triangles in Fig. 1b), so we tested whether the mortality risk increase could be due to cyclone occurrence alone. We performed two re-analyses of the full model construction using a) all plots, but with any census interval with observed cyclone occurrence removed, and b) only plots with no cyclone disturbances in the past 50 years. In both cases, there remained a marked increase in mortality risk across years following 1984 (Fig. S4, Table S6), suggesting that another mortality cause was driving, and possibly interacting with wind disturbance events, to increase mortality risk across the plots.

To evaluate whether some taxa were particularly vulnerable to changing climate, we tested how species mortality risks changed after 1984 in model M4, and examined how their local distributions related to their total geographic range (model M5), and if some traits correlated with their average mortality risk or rate of mortality risk increase (model M6). Model M4 confirmed a general increase in mortality risk over time across species (β_0 = 0.17 [0.21, 0.14]; Fig. 4a,b, Table S4), with 70% of the species presenting the trend (Fig. 3b) and substantial variability across species (σ_β: 0.19 [0.16, 0.21], see eqs. 4) (Fig. 3b). Species average annual mortality risk varied between 0.007 and 0.051 (mean of 0.021; Table S2).

Although the increasing mortality trend across species and plots in our analysis is clear, attributing this trend to specific causes is challenging. Mortality can lag its cause by months to years [32–36] and any single mortality event can be due to multiple interacting causes [33,35,37–39]. Available meteorological data cannot perfectly capture the mortality mechanisms due to spatial and temporal precision, or accurate representation of the driving mechanism (i.e., the disconnect between high VPD, embolism, vascular failure, and crown death). Finally, observations of mortality in censuses do not represent the exact year of death. We attempted to extend our inference from the observed mortality risk pattern to possible attribution in three ways: (1) linking geographical ranges to plot-level patterns among species, (2) testing trait relationships to the mortality shift, and (3) investigating cyclone occurrence and the plot- and species-specific mortality risk trends.

Many of the species in our plots are widespread across tropical southeast Asia, offering a robust assessment of climate niche. Climate niches were approximated for 56 of the 81 species that occurred in at least four of the 24 plots, using a projection of presences across climate space built by combining all recorded species occurrences with a 30-year climatology of maximum VPD, temperature, and MCWD. We then expressed each of our plot mean climate metrics in terms of quantiles on each species' total univariate climatic niche, yielding variables of study species position on their broader geographical climate niche (VPD_{niche}, $Tmax_{niche}$, $MCWD_{niche}$; Fig. 4). Model M5 regressed mortality risk after 1984 on these three niche-related covariates, with 'year' to control for the temporal increase and with species-level slopes for all covariates (see eqs. 5). The average mortality risk was higher the closer species were to the drier edge of their range (i.e. upper limit of their VPD niche; $\beta_{3,0}$: 0.40 [0.27, 0.52]; Figs. 2, 4, Table S5). This increase of average mortality risk with VPD_{niche} affected 79% of the 56 species (Fig. 4). A similar, though-less-marked, increase in average mortality risk occurred closer to the upper edge of the $Tmax_{niche}$ when considering a 90%-HPDI ($\beta_{2,0}$: 0.13 [0.01, 0.24]; eqs. 5). This $Tmax_{niche}$ effect increased when removing VPD_{niche} from the model, indicating that $Tmax_{niche}$ is associated with mortality risk indirectly through VPD_{niche} (see sensitivity analysis in Supp. Methods S1 and Table S5). The position on the MCWD niche had no clear effect across species (Table S4).

Functional traits may indicate distinct mortality vulnerabilities among species. Forty of our study's species had functional trait measurements, including morpho-anatomical features such as leaf mass per area and wood density, chemical traits such as leaf C stable isotope ratio, leaf nitrogen and phosphorus, and gas exchange traits such as stomatal conductance and maximum photosynthetic capacity (Table S7, Fig. S5). To test for physiological mechanisms potentially underlying interspecific differences in the pace of mortality risk change over time, we used the subset of 40 species with trait data in a modified version of M4 to see if species mean trait values predicted a species' average risk and the temporal change in that risk post 1984 (models M6, Table S4). Wood density (a proxy for mechanical strength and embolism resistance [40,41]) showed a clear negative relationship with average mortality risk (α_1: -0.21 [-0.38, -0.05]; eqs. 6). No traits, however, predicted the variation among species in the temporal change (i.e. the slope) of the mortality risk (Fig. 2, Fig. S6). This lack of a signal could be due to using species average traits or limited sample sizes in focusing on species across plots as well as the potential for a null or minor effect [33,42].

Wind damage contributes to tree mortality and carbon cycling in other tropical forests [43–45], and the prevalence of cyclone impacts recorded in a number of plots here indicate that wind may have contributed to the increase in mortality risk directly or indirectly. Whereas wind-related events often determine the moment of tree death, other abiotic and biotic risk factors are key in determining tree vulnerability to storms, highlighting the importance of interactions among multiple risk factors in determining tree death [21,33,35,39]. In particular, VPD is likely to increase tree vulnerability to wind damage, as well as to other risk factors such as biotic agents [33,35], in addition to its direct water-related stress [16,46].

Mortality changes in tropical forests have been associated with climate events such as droughts, which will impact long-term forest dynamics if they become more pervasive [1,47,48]. Here, MCWD did not explain average mortality risk across plots nor showed any clear temporal trend associated with mortality risk (Fig. S11, Bauman et al. [23]). Further exploring how chronically increasing VPD (presses [49]) interacts with heat waves, drought events and more frequent extreme VPD anomalies (pulses [49]) to affect long-term mortality trends will be important to better quantify a causal link between climate change and tree mortality. Our study indicates, whether due to particular events or accumulated vulnerability, a consistent increase in mortality. When compounded over large areas for long periods of time, this mortality increase can result in changes in forest dynamics, structure, composition, and carbon residence time [31,50]. Increasing a typical tree mortality rate from 1% to 2% per year, for instance, halves tree life expectancy, carbon residence time and, in the absence of increases in forest-wide productivity, long-term biomass stocks [31].

To test potential impacts of the mortality increase on stand structure, we tested whether decreases in plot-level basal area (BA; as a proxy for above-ground biomass) were offset by subsequent BA increases due to growth and recruitment into the census. We found a clear decline in BA over the monitoring period, in line with Murphy et al. [51] (Fig. 3c,d; Fig. S7). The change in BA between censuses (i.e., drops or gains) showed an increasing number and extent of drops (Fig. 3c), and these were not offset by gains (Fig. 3c,d). Over the period studied, plots lost ~230.2 m^2 ha^{-1} but gained only 113.7 m^2 ha^{-1}, a 12.2% decline from the BA of the first census of each plot, converting these forests into biomass carbon sources. Although some studies have suggested that large trees are more vulnerable to water stress due to height-driven hydraulic extension, which could have disproportionate consequences for biomass change [13,52], we found no evidence of this here (Fig. S8), in line with recent works [33].

Our study shows that (1) mortality risk increased across plots and species, (2) tropical cyclones alone cannot explain the pattern, (3) average mortality risk is higher in drier plots and at the drier edge of most species geographical ranges, (4) VPD displays a temporal increase in all plots that corresponds to the mortality risk increase (unlike MCWD), and is a known physiological stressor and mortality risk factor [8,16], and (5) there is no evidence that the mortality risk increase is driven by increases in growth rates (see Supp. Methods S1; Fig. S9). Tree growth was also recently shown to be reduced by positive VPD anomalies in the region, with fast-growing species as well as drier plots being more suppressed [23]. While acknowledging the contribution of wind disturbances and other unaccounted for mortality risk factors such as lightning, the above elements provide evidence that a chronic long-term increase in atmospheric evaporative demand may increase mortality risk in moist tropical forests of Australia. This is supported by similar findings in the Amazon and African tropical forests [1,2] and when comparing key climate variables across our plots to the climate of moist tropical forest globally: VPD, Tmax, annual precipitation and climatic water deficit at our plots encompassed 53%, 18%, 78%, and 31% of global-scale tropical moist forest climatic space, respectively (Fig. S10). The near ubiquitous nature of temperature and VPD rise across the tropics suggests that this phenomenon may be responsible for, and may in the future drive, an acceleration of tree mortality and concomitant decrease of living biomass across the tropics.

One potential buffer to climate change impacts on diverse forests could be the variety of ways different species tolerate shifts in the conditions that lead to water [53,54] or temperature stress [55]. These strategies may be represented by species functional traits [13,41,54]. Higher wood density correlated with reduced average annual mortality risk, indicating potential roles for enhanced wood strength or resistance to embolism [40,41]. Here, none of the measured traits explained the interspecific variation in the temporal increase in mortality risk. However, we cannot rule out that other traits (e.g., hydraulic safety margin and xylem vulnerability to embolism [5,33,54]) might better explain mortality risk changes across species. Australian moist tropical forest species, in particular, have been shown to have narrower hydraulic safety margin than species growing in drier forests [41].

Some of the challenges in attributing mechanisms to mortality observations are unavoidable, such as the lag between cause and consequence of death, but intensified monitoring protocols and new technologies should improve attribution [35,38,56]. In addition to long-term plot monitoring, mortality attribution can be improved with focused collections of environmental stressors at high

frequency (e.g., micrometeorology, soil moisture at depth), as well as higher-frequency monitoring individual tree death (e.g., annual or even seasonal mortality surveys [35,38,56]). Better assessment of tree health through methods as focused as sap flux or as broad as remote sensing of leaf function, could also improve our ability to assign cause to individual mortality events. Such intensified monitoring programs should improve representation of mortality risk in vegetation models, a crucial advance to better predict the future pathway of the tropical forest carbon sink, and hence the remaining anthropogenic carbon budget available to stay well below 2 °C peak global warming.

References

1. Brienen, R. J. W. *et al.* Long-term decline of the Amazon carbon sink. *Nature* **519**, 344–348 (2015).
2. Hubau, W. *et al.* Asynchronous carbon sink saturation in African and Amazonian tropical forests. *Nature* **579**, 80–87 (2020).
3. Zuleta, D., Duque, A., Cardenas, D., Muller-Landau, H. C. & Davies, S. J. Drought-induced mortality patterns and rapid biomass recovery in a terra firme forest in the Colombian Amazon. *Ecology* **98**, 2538–2546 (2017).
4. Phillips, O. L. *et al.* Drought sensitivity of the Amazon rainforest. *Science* **323**, 1344–1347 (2009).
5. Powers, J. S. *et al.* A catastrophic tropical drought kills hydraulically vulnerable tree species. *Glob. Chang. Biol.* **26**, 3122–3133 (2020).
6. Bennett, A.C. *et al.* Resistance of African tropical forests to an extreme climate anomaly. *Proc. Natl. Acad. Sci. U. S. A.* (2021).
7. Brodribb, T. J., Powers, J., Cochard, H. & Choat, B. Hanging by a thread? Forests and drought. *Science* **368**, 261–266 (2020).
8. McDowell, N. G. *et al.* Pervasive shifts in forest dynamics in a changing world. *Science* **368**, (2020).
9. Pan, Y. *et al.* A large and persistent carbon sink in the world's forests. *Science* **333**, 988–

993 (2011).

10. Matthews, H. D. *et al.* An integrated approach to quantifying uncertainties in the remaining carbon budget. *Comm. Earth. Environ.* **2**, e7 (2021).
11. Girardin, C. A. J. *et al.* Nature-based solutions can help cool the planet — if we act now. *Nature* **593**, 191–194 (2021).
12. Choat, B. *et al.* Triggers of tree mortality under drought. *Nature* vol. 558 531–539 (2018).
13. Rowland, L. *et al.* Death from drought in tropical forests is triggered by hydraulics not carbon starvation. *Nature* **528**, 119–122 (2015).
14. Lloyd, J. & Farquhar, G. D. Effects of rising temperatures and [CO2] on the physiology of tropical forest trees. *Philos. Trans. R. Soc. Lond. B Biol. Sci.* **363**, 1811–1817 (2008).
15. O'sullivan, O. S. *et al.* Thermal limits of leaf metabolism across biomes. *Global Change Biology* vol. 23 209–223 (2017).
16. Grossiord, C. *et al.* Plant responses to rising vapor pressure deficit. *New Phytol.* **226**, 1550–1566 (2020).
17. Rifai, S. W., Li, S. & Malhi, Y. Coupling of El Niño events and long-term warming leads to pervasive climate extremes in the terrestrial tropics. *Environ. Res. Lett.* **14**, 105002 (2019).
18. Rifai, S. W. *et al.* ENSO Drives interannual variation of forest woody growth across the tropics. *Philos. Trans. R. Soc. Lond. B Biol. Sci.* **373**, (2018).
19. Smith, M. N. *et al.* Empirical evidence for resilience of tropical forest photosynthesis in a warmer world. *Nat. Plants* vol. 6 1225–1230 (2020).
20. Malhi, Y. *et al.* Exploring the likelihood and mechanism of a climate-change-induced dieback of the Amazon rainforest. *Proc. Natl. Acad. Sci. U. S. A.* **106**, 20610–20615 (2009).
21. McDowell, N., Allen, C. D. & Anderson-Teixeira, K. Drivers and mechanisms of tree mortality in moist tropical forests. *New Phytol.* **219**, 851–869 (2018).
22. McDowell, N. *et al.* Mechanisms of plant survival and mortality during drought: why do some plants survive while others succumb to drought? *New Phytol.* **178**, 719–739 (2008).

23. Bauman, D. *et al.* Tropical tree growth sensitivity to climate is driven by species intrinsic growth rate and leaf traits. *Glob. Chang. Biol.* **28**, 1414–1432 (2022).
24. Esquivel-Muelbert, A. *et al.* Tree mode of death and mortality risk factors across Amazon forests. *Nat. Commun.* **11**, 5515 (2020).
25. Anderegg, W. R. L., Anderegg, L. D. L., Kerr, K. L. & Trugman, A. T. Widespread drought-induced tree mortality at dry range edges indicates that climate stress exceeds species' compensating mechanisms. *Glob. Chang. Biol.* **25**, 3793–3802 (2019).
26. Aguirre-Gutiérrez, J. *et al.* Drier tropical forests are susceptible to functional changes in response to a long-term drought. *Ecol. Lett.* **22**, 855–865 (2019).
27. Aguirre-Gutiérrez, J. *et al.* Long-term droughts may drive drier tropical forests towards increased functional, taxonomic and phylogenetic homogeneity. *Nat. Comm.* **11**, 1–10 (2020).
28. Meir, P., Mencuccini, M. & Dewar, R. C. Drought-related tree mortality: addressing the gaps in understanding and prediction. *New Phytol.* **207**, 28–33 (2015).
29. Sullivan, M. J. P. *et al.* Long-term thermal sensitivity of Earth's tropical forests. *Science* **368**, 869–874 (2020).
30. Yuan, W. *et al.* Increased atmospheric vapor pressure deficit reduces global vegetation growth. *Sci. Adv.* **5**, eaax1396 (2019).
31. McMahon, S. M., Arellano, G. & Davies, S. J. The importance and challenges of detecting changes in forest mortality rates. *Ecosphere* **10** e02615 (2019).
32. Trugman, A. T. *et al.* Tree carbon allocation explains forest drought-kill and recovery patterns. *Ecol. Lett.* **21**, 1552–1560 (2018).
33. Trugman, A. T., Anderegg, L. D. L., Anderegg, W. R. L., Das, A. J. & Stephenson, N. L. Why is Tree Drought Mortality so Hard to Predict? *Trends Ecol. Evol.* **36**, 520–532 (2021).
34. Phillips, O. L. *et al.* Drought-mortality relationships for tropical forests. *New Phytol.* **187**, 631–646 (2010).

35. Aleixo, I. *et al.* Amazonian rainforest tree mortality driven by climate and functional traits. *Nat. Clim. Change* **9**, 384–388 (2019).
36. Lingenfelder, M. & Newbery, D. M. On the detection of dynamic responses in a drought-perturbed tropical rainforest in Borneo. *Plant Ecol.* **201**, 267–290 (2009).
37. McDowell, N. G. *et al.* The interdependence of mechanisms underlying climate-driven vegetation mortality. *Trends Ecol. Evol.* **26**, 523–532 (2011).
38. Zuleta, D. *et al.* Individual tree damage dominates mortality risk factors across six tropical forests. *New Phytol.* **233**, 705–721 (2022).
39. Fontes, C. G. *et al.* Dry and hot: the hydraulic consequences of a climate change-type drought for Amazonian trees. *Philos. Trans. R. Soc. Lond. B Biol. Sci.* **373**, (2018).
40. Chave, J. *et al.* Towards a worldwide wood economics spectrum. *Ecol. Lett.* **12**, 351–366 (2009).
41. Peters, J. M. R. *et al.* Living on the edge: A continental-scale assessment of forest vulnerability to drought. *Glob. Chang. Biol.* **27**, 3620–3641 (2021).
42. Yang, J., Cao, M. & Swenson, N. G. Why Functional Traits Do Not Predict Tree Demographic Rates. *Trends Ecol. Evol.* **33**, 326–336 (2018).
43. Espírito-Santo, F. D. B. *et al.* Size and frequency of natural forest disturbances and the Amazon forest carbon balance. *Nat. Commun.* **5**, 3434 (2014).
44. Chambers, J. Q. *et al.* The steady-state mosaic of disturbance and succession across an old-growth Central Amazon forest landscape. *Proc. Natl. Acad. Sci. U. S. A.* **110**, 3949–3954 (2013).
45. Rifai, S. W. *et al.* Landscape-scale consequences of differential tree mortality from catastrophic wind disturbance in the Amazon. *Ecol. Appl.* **26**, 2225–2237 (2016).
46. López, J., Way, D. A. & Sadok, W. Systemic effects of rising atmospheric vapor pressure deficit on plant physiology and productivity. *Glob. Chang. Biol.* **27**, 1704–1720 (2021).
47. Brando, P. M. *et al.* Abrupt increases in Amazonian tree mortality due to

drought\textendashfire interactions. *Proc. Natl. Acad. Sci. U.S.A.* **111**, 6347–6352 (2014).

48. Phillips, O. L. *et al.* Pattern and process in Amazon tree turnover, 1976-2001. *Philos. Trans. R. Soc. Lond. B Biol. Sci.* **359**, 381–407 (2004).
49. Harris, R. M. B. *et al.* Biological responses to the press and pulse of climate trends and extreme events. *Nat. Clim. Change* **8**, 579–587 (2018).
50. Andrus, R. A., Chai, R. K., Harvey, B. J., Rodman, K. C. & Veblen, T. T. Increasing rates of subalpine tree mortality linked to warmer and drier summers. *J. Ecol.* **109**, 2203–2218 (2021).
51. Murphy, H. T., Bradford, M. G., Dalongeville, A., Ford, A. J. & Metcalfe, D. J. No evidence for long-term increases in biomass and stem density in the tropical rain forests of Australia. *J. Ecol.* **101**, 1589–1597 (2013).
52. Bennett, A. C., McDowell, N. G., Allen, C. D. & Anderson-Teixeira, K. J. Larger trees suffer most during drought in forests worldwide. *Nat. Plants* **1**, 1–5 (2015).
53. Chitra-Tarak, R. *et al.* Hydraulically-vulnerable trees survive on deep-water access during droughts in a tropical forest. *New Phytol.* **231**, 1798–1813 (2021).
54. Anderegg, W. R. L. *et al.* Meta-analysis reveals that hydraulic traits explain cross-species patterns of drought-induced tree mortality across the globe. *Proc. Natl. Acad. Sci. U. S. A.* **113**, 5024–5029 (2016).
55. Taylor, T. C., Smith, M. N., Slot, M. & Feeley, K. J. The capacity to emit isoprene differentiates the photosynthetic temperature responses of tropical plant species. *Plant Cell Environ.* **42**, 2448–2457 (2019).
56. Arellano, G., Zuleta, D. & Davies, S. J. Tree death and damage: A standardized protocol for frequent surveys in tropical forests. *J. Veg. Sci.* **32**, e12981 (2021).

Figure legends

Figure 1: Temporal increase of modelled annual mortality risk, annualised observed percentage of tree death, and atmospheric vapour pressure deficit across the 24 studied plots. a: Temporal variation of the modelled latent mortality risk per year across all 24 plots and 81 species, with a change-point identified in 1984 marking the beginning of an increase (see Table S3). Circles and intervals are median and 95%-highest posterior density intervals of the year-level mortality risk (see M2, Table S4). b: Annualised percentage of tree death per plot and census interval, indicating a temporal increase across all plots, partly but not only related to wind damage from cyclones (black triangles). c: Predicted temporal increase of maximum annual vapour pressure deficit (VPD) across all 24 plots. Line and shaded areas are median and 95%-highest posterior density intervals (HPDI) for VPD predicted from the model fit (see Methods).

Figure 2: Temporal increase of tree mortality risk and influence of plots' mean climate, species' position on their climatic niche, and functional traits on mortality risk. Results displayed from the Bayesian multilevel models M3 to M6 investigating different aspects of the mortality risk pattern (Table S4). Red and blue arrows represent clear negative and positive effects on mortality risk, respectively, while grey arrows indicate that no clear effect was detected (i.e. slope coefficients whose posterior 95%-highest posterior density intervals, HPDI, encompasses zero). Plain and dashed arrows illustrate direct and indirect effects on tree mortality risk respectively, where indirect effects affect mortality risk by accentuating or attenuating the direct effect of 'year' (details in Supp. Methods S1). VPD: vapour pressure deficit. MCWD: Maximum climatological water deficit. Tmax: Maximum daily air temperature. WD: Wood density. Coefficients from different models cannot be directly compared, as they arise from models using different subsets of the dataset (see Methods; Table S4). Palm vector created by kjpargeter - www.freepik.com.

Figure 3: Plot- and species-level temporal changes of annual mortality risk (1984-2019) and change of plot basal area between consecutive censuses. a,b: Circles and intervals are median and 95%-highest posterior density intervals (HPDI) of plot-level (a) and species-level (b) 'year' slope coefficient posteriors (β_k and β_j, respectively; see eqs. 3 and 4), from models M3 and M4, respectively. Plots and species whose 95%-HPDI encompassed zero are half-transparent. Blue and red circles indicate clear temporal increases and decreases in mortality risk, respectively, at a 95% level of confidence (HPDI). The black vertical solid and dashed lines are the median and 95%-HPDI of the grand 'year' slope (i.e. 'year' effect across plots (a) and species

(b); β_0 in eqs. 3 and 4). Insets: Model prediction of mortality risk per year for the period 1984-2019, showing the median (line) and 95%-HPDI (shaded area) of the posterior distributions for the grand effect. Model posterior predictions show ca. a doubling of mortality risk between 1984 and 2019 (2.1-fold and 1.7-fold increases at plot- and species level, respectively). c: Variation of ΔBA per plot over time, where ΔBA is the change of basal area between consecutive censuses in a given plot ($\Delta BAt = BA_t - BAt_{-1}$), such that positive values indicate an increase in BA from census t - 1 to census t, and negative values indicate a decrease. Each circle is the ΔBA of a plot at the beginning of a census period, and lines connect consecutive observations for each plot. d: Density distribution of the annualised ΔBA based on consecutive plot censuses, before and after the change-point of 1984. Figs. c and d show that BA losses due to mortality were not offset by BA gains related to growth and recruitment into the census.

Figure 4: Spatial effect of species' proximity from the upper limit of their VPD niche on average mortality risk (model M5). The upper part of the figure illustrates for one species (*Cryptocarya densiflora Blume*) the calculation of species' VPD niche quantiles (VPD_{niche}) in the study plots where the species occur (red circles), on the basis of its total biogeographic distribution (sum of black and red circles), its climatic niche calculated based on 30-year climatology (map background) of the locations where the species was observed (density plot), and the mean VPD_{max} in the studied plots where the species is (red bars at bottom of density plot). The lower part of Fig. 4 shows the effect of VPD_{niche} on average mortality risk per species and across species (vertical solid and dashed lines; see legend of Fig. 3 for circles and bars, and eqs. 5 in Supp. Methods S1 for model details). Species at the upper end of their VPD niche are more likely to experience increased mortality risk.

Methods

Site and species data: The dataset encompasses 49 years of inventory data from 24 tropical rainforest plots distributed along an elevation gradient ranging between 15 and 1500 m a.s.l., and censused on average 12 times, in northern Queensland, Australia, between -12.73 to -21.25 and 143.25 to 148.55 (see details in Table S1 and [23]). Each census consisted of the measurement of all trees above 10 cm diameter at breast height (DBH). Twenty plots (0.5-ha, 100 × 50 m) were established between 1971 and 1980 to provide long-term ecological and demographic data [57], while four plots were established more recently along the same elevation gradient (Table S1).

With two exceptions, the plots were established in unlogged forest; at establishment, EP9 and EP38 showed localised evidence of disturbance due to selective logging at least 20 years prior [57]. Cyclonic disturbance contributes to the dynamics of the forests [51], with at least one plot affected by cyclones in 1986, 1989, 1999, 2006, 2011, 2014, 2017, and 2019 (Fig. 1b). The gradient covers a wide range of mean annual temperatures (19°C to 26.1°C), precipitation (1213 to 3563 mm), and mean vapour pressure deficit (6.5 to 11.8 hPa) (Table S1). All trees with stems ≥ 10 cm diameter at breast height (DBH) were mapped, identified to species level and measured for diameter. The 20 long-term plots were re-measured every two years for ten years, and then at three- to four-year intervals, with diameter, recruits and deaths recorded, summing up to 11 to 17 censuses per plot. The remaining four plots were established more recently, between 2001 and 2012, and were resampled one to three times (Table S1).

The initial dataset comprised 110,551 observations, from 13,513 individual stems from 535 species, in 54 genera, and 79 families (details in Table S2 of Bauman et al. [23]). We used a cutoff of a minimum of 400 observations per species to model the functional size-dependence of survival of a species (see Data analysis), to ensure sufficient statistical power (species list and sampling features in Table S2). This resulted in a dataset of 81 tree species, 8,314 individual stems, 74,135 observations, and 492 death events over the 49 years across the 24 forest plots. Species were found in between 1 to 16 plots, with a mean of 6.1, and individual stems were censused two to 17 times (mean 10.4) over periods of two to 44 years (mean: 13 years) (Table S2).

Estimating tree survival across size, space, and time: The basis of all downstream analyses was the estimation of the yearly probability of survival (a latent, or unobserved, variable) from fitting a survival function to each species separately in a multilevel model framework, with 'plot' and 'year' as varying effects (also often referred to as 'random effects'). The first step of our approach consisted of estimating size-dependent tree survival by fitting a functional form to every species separately, across the multiple censuses and forest plots where it occurred. The model we developed to characterise tree survival built upon recent work by Johnson et al. [58] and Needham et al. [59], combining the same five survival parameters into an S- and inverse S-shaped logistic function of survival probability (Fig. S1; eqs. 1.4, 1.5; see model details in Supp. Methods S1). These correspond to the baseline survival probability per year (K; survival probability for most of the adult life of an individual), the rate of survival increase until reaching the arbitrary size where the survival probability becomes K ($r1$), the size corresponding to the inflexion point of the first S-shaped portion of the functional form ($p1$), and the corresponding $r2$ and $p2$ parameters for the inverse-S-shaped portion of the functional form, corresponding to the yearly rate of survival

decrease when the species approaches its maximum size, and the inflexion point corresponding to the size at which the yearly survival probability is 50% (species stature), respectively (Fig. S1; illustration for four species in Fig. S2).

In this study, we sought to investigate temporal changes in the survival probability per year (*K*) over the past 50 years, whether they vary across space (forest plots along a climatic gradient) and species, and test whether long-term climate, species' biogeographic range, and species traits mediate these temporal patterns.

For each species separately, we modelled the logit-scaled *K* as a function of a species-specific mean K (K_μ) from which deviations arise from different plots (*K_P*) and years (*K_T*) (Fig. S1; eq. 1.2). Instead of modelling the survival rate over the actual census period (mostly between two to five years, see [23]), we took advantage of having different plots whose starting and ending census years differed and partly overlapped (Fig. 1b) to generate a latent variable of logit-scaled probability of survival K per plot and year (hereafter *K_lat*, Fig. 1; eq. 1.2). The real observations of binary survival outcomes (eq. 1.1) per stem per census t were thus used to generate latent probabilities of survival for every year encompassed by the period between consecutive censuses. Our Bayesian framework allowed estimating a posterior distribution of *K_lat* for each latent observation (i.e. stem per plot per year; Fig. S9), as:

$$Survival_{i,k,t} \sim Bernoulli(\theta) \quad (1.1)$$ [Likelihood of survival for obs. *i* in plot *k*, interval *t*]

$$for\ (x\ in\ year\_0_i : year\_1_i)\ \{$$ [Loop through years encompassed by the time interval]

$$K\_lat = K\_\mu + K\_P_i + K\_T_{i,x} + \epsilon_i \quad (1.2)$$ [Latent logit-survivorship per year]

$$K = inv\_logit(K\_lat) \quad (1.3)$$ [Inverse logit of latent survivorship per year]

$$\theta = \begin{cases} \frac{K}{1+exp^{(-r1\times(dbh_i-p1))}},\ dbh_i < threshold & (1.4) \\ \frac{K}{1+exp^{(-r2\times(dbh_i-p2))}},\ dbh_i \geq threshold & (1.5) \end{cases}$$ [Logistic functions of survival]

}

$$K\_\mu \sim Normal(2,1) \quad (1.6)$$ [Prior for average logit-survivorship]

$$K\_P \sim Normal(0,\sigma_P) \quad (1.7)$$ [Adaptive prior for plots]

$$K\_T \sim Normal(0,\sigma_T) \quad (1.8)$$ [Adaptive prior for years]

$$\epsilon \sim Normal(0,\sigma_\epsilon) \quad (1.9)$$ [Adaptive prior for residual error]

where survival outcomes were modelled through either one of the logistic functions corresponding to the S-shaped or inverse S-shaped functions (eqs. 1.4 and 1.5, respectively), depending on whether the corresponding individual presented a DBH smaller or bigger than a threshold, here set as the mean DBH of the species (see Supp. Methods S1 for prior specifications).

We extracted the median of the *K_lat* posterior distribution per latent observation (i.e. survival probability of a given stem on a given year). The resulting distribution of median *K_lat* values combined across all 81 species and 24 plots was used as the main response variable in the following models to investigate temporal patterns of survival.

We focus on the variation across groupings (species, plot and year) with *K_lat* as it best summarises mortality of trees through most of their lives (Figs. S7, S8). Although the other parameters that offer insights into early and late mortality are very powerful for certain questions, allowing that the data are available, we decided against focusing on differential mortality of small individuals due to the minimum size threshold of 10 cm DBH, a size above which most stems function similarly (i.e., seedling and sapling drought vulnerability would fall well below this threshold). We do, however, acknowledge that non emergent trees above 10 cm DBH may experience buffered variations in VPD and other variables related to their below canopy position, which we do not account for here.

All following analyses were performed on the latent logit-survivorship (*K_lat*), model results and coefficients are reported in terms of mortality probability (hereafter "mortality risk"), where annual mortality risk is defined as 1 - survival probability, and the coefficient signs from the models presented below had their sign inverted (e.g. a negative effect on survivorship becomes a positive effect on mortality risk). Note that as our approach focuses on linking mortality to ontogeny through size, it precludes accounting for census-interval length biases that emerge when longer intervals miss mortality events of individuals that grow into the census diameter and die before being recorded [60]. As these biases will tend to increase mortality estimates for shorter census interval lengths and become more pronounced for smaller size classes, our study has, if anything, underestimated mortality after the census interval increased in the early 1980's (see Fig. 1b).

Statistical analyses

Our statistical analyses followed from our initial hypotheses about tropical forest survival patterns, but also from our initial findings as related to those patterns. Therefore, our analysis proceeded through different models that relied on different subsets of the data depending on the questions asked. We began by investigating trends in mortality risk across plots and species and then focused on aspects that included species subsets occurring in multiple plots, plot communities independent of species, and biogeographic inference about the species across the plots. The six models used are summarised in Table S4 and the next section (detailed model explanations and all equations are in Supp. Methods S1). Because mortality events are rare and stochastic,

requiring a lot of data for inference, and because the six models have different requirements (see below), we settled on maximising inference from each model over reducing the data set to the smallest common dataset allowing model comparison at the cost of statistical power. Different subsets of the data were therefore used for models M3 to M6 (see Tables S2, S4).

Temporal trends in survival: We first generated an unconditional multilevel model of *K_lat* across all 81 species (model M1 in Table S4), for a visual assessment of a temporal trend in the average survivorship per year (see eqs. 2 for model details in Suppl. Methods S1). M1 used varying intercepts (also known as "random" intercepts) to model mortality risk (*K_lat*; i.e. overall intercept, or grand mean) and species-level, plot-level and year-level deviations from the grand mean. Because an increasing trend in tree mortality risk was apparent in the 1980s (Fig. 1a), we tested for a changepoint year.

Changepoint: We used a changepoint analysis to statistically test whether our time series of latent logit-survival probabilities (*K_lat*) has shifted in mean value and, if so, to identify the most likely year when this change occurred [31,61] (model M2, Table S4). A change point from slightly negative to clearly positive temporal trend in mortality risk was identified in 1984, across all plots and species (Fig. 1a). All further analyses focused on the structure and potential causes of the increase in tree mortality risk in the 1984-2019 35-year period.

Explaining the 'post-change point' survivorship decline: Causes of individual tree mortality are difficult to assess directly due to time lags between mortality and its cause, tree deaths being most often attributable to multiple mechanisms [33,39,62–64], and delays between the mortality event and its detection [35,65,66]. Because of this, direct causal relationships between tree mortality and specific weather events or average climatic conditions of a census interval are not possible. Instead, we use different datasets and approaches in order to best attribute known potential drivers of tree mortality with the patterns identified in the long-term data.

Plot-level changes and local mean climate: We built a Bayesian hierarchical model exploring the post-1984 mortality risk increase within and across plots to test the proportion of plots showing an increase in mortality risk through time, and to test whether average mortality risk and mortality risk changes over time depended on the local mean climate (model M3 in Table S4; details in eqs. 3, Supp. Methods S1). To do so, we used plot mean climate, defined as a 35-year local average per climatic variable (1984-2019, to match the main period of interest). We specifically

considered the effect of the 30-year average of the VPD of the year driest quarter and maximum temperature of the year warmest quarter (Tmax) as both VPD and temperature have markedly increased in all 24 plots during the past 49 years and are important drivers of tree growth in these plots [23]. Additionally, we examined the effect of maximum climatological water deficit (MCWD), a metric that serves as a proxy for the annual accumulated water stress over the dry season estimated as the cumulative deficit between precipitation and evapotranspiration [20,67,68]. These variables can all have an impact on survival through water stress or heat-related impairment of biochemical reactions (which are not captured explicitly in this study). The VPD and temperature data were collected from ANUClimate v.2.0 between 1971 and 2019 [69], and the MCWD was calculated using precipitation data from ANUClimate v.2.0 and evapotranspiration data from TerraClimate [70].

Species-level changes and biogeographic expectations: We used a similar Bayesian multilevel model specification as the previous one, without climate variables, to focus on species-specific mortality risk change trajectories and test the proportion of species showing an increase in mortality risk over time (model M4; Table S4).

We then used a space-for-time substitution to test whether the temporal increase in mortality risk could be driven by the marked temporal increase of temperature and VPD (see Results). Specifically, we tested whether species had lower average survival rates in plots closer to the drier edge of their geographical range (upper limit of their total VPD niche). Similarly, MCWD was used to approximate species' rainfall seasonality niche. This approach takes into account general eco-physiological constraints as well as the evolutionary history of each species, as captured through the biogeographic range of conditions where they occur [71,72]. For example, a difference of 2°C in the mean temperature of two plots could be associated with a higher baseline mortality for one species for which the warmer plot falls close to the edge of its temperature niche, whereas baseline mortality would remain the same for a species for which both plots are near the species' niche center. This biogeographic niche approach allowed us to investigate potential mechanisms underlying temporal trends [73], while also providing potential eco-physiological mechanisms underlying the temporal and spatial pattern [72,74,75].

To generate approximate univariate climate niches for each species and define the relative location of the studied plots in these niches, we first extracted all known occurrences of 78 species (see next section) from the Global Biodiversity Information Facility (GBIF) online database (Table S8). Our goal was to balance the simplicity of a presence-only analysis while avoiding biases that might underestimate niche breadth. We therefore first filtered out multiple occurrences of a

species to keep only one sample per radius of 1 km, to reduce the risk of oversampling [76] (a 3 km radius filter yielded very similar results; results not shown). The filtered spatial locations of the 78 species occurrences were matched to a 1/24° map of the 30-year climatology (average over 1981-2010) of maximum annual VPD, maximum daily air temperature (Tmax), and MCWD, obtained from TerraClimate [70]. Species' univariate climate niches were defined separately for Tmax, VPD and MCWD as the distribution of 30-year mean values from the pixels corresponding to each species' biogeographic distribution (including our plots) (see upper part of Fig. 4). The local 30-year average climate of our 24 plots were then expressed in terms of quantiles for each species separately, based on the species-specific climatic niches generated, yielding $Tmax_{niche}$, VPD_{niche}, and $MCWD_{niche}$, that is, species' position on their total niche for the corresponding variable. The resulting quantiles are species-specific expressions of how close the 30-year mean climate variables in our plots are from the upper limit of species' total climatic niche. We tested the robustness of our quantile approach with respect to potential imperfect sampling in part of the biogeographic area by rerunning the M5 model using a coarser index of the distance from the niche maximum expected to show little sensitivity to uneven sampling effort across species' total distribution area (details in Supp. Methods S1).

Species-level changes and functional traits: To investigate potential eco-physiological mechanisms underlying the species-level variability in the post-1984 change of survivorship through time, we used a modified version of model M4 only considering the 40 species with measured functional trait data (M6, Table S4), instead of all 81 species. Model M6 allowed testing whether the differences in both average mortality risk and the pace of risk change over time could be explained by species traits (model details in Supp. Methods S1).

The functional traits were measured between July and September 2015 on 81 dominant, canopy trees in seven of the 24 plots (Table S7; Table S1 and S2 for plots and species with trait data). For each plot, species were chosen with the aim of sampling those that made up 80% of the standing biomass for the most recent census. The details of trait data collection and measurements are presented in Bauman et al. [23] and are summarised here. Measured traits and their functions are presented in Table S3 and Fig. S5. The traits were measured on three individuals per species, and included leaf photosynthesis and stomatal conductance at a reference CO_2 concentration of 400 μmol mol^{-1} and irradiance of 1500 μmol photons m^{-2} s^{-1} (Asat and gsat, respectively), dark respiration (Rd) at the same CO_2 concentration, the CO_2-saturated photosynthesis and stomatal conductance (Amax and gmax), measured at 1200 μmol mol^{-1} CO_2. Estimates of leaf maximum carboxylation rate (Vcmax) and maximum light-driven electron flux

(Jmax) normalized to 25°C were obtained from the photosynthesis model of Farquhar et al. [77] fitted to the *A*-c_i curves ('*plantecophys'* R package [78]). The one-point method [79] was used to estimate Vcmax for each individual from net photosynthesis measured at 400 μmol mol^{-1} CO_2, and Jmax from net photosynthesis measured at 1200 μmol mol^{-1} CO_2 [80]. We also measured leaf area, leaf mass per area (LMA), leaf thickness, wood density (from branches, after bark removal), leaf nutrient concentrations, and stable carbon isotope ratio ($\delta^{13}C$). All traits were averaged at the species level for the analyses.

Sensitivity analyses for the risk trend: We ran four sensitivity analyses to test the robustness of the temporal trend in mortality risk increase after removing major influences of wind damage-related disturbances from cyclones. To do so, we created two subsets of the initial raw survival dataset by filtering out (1) any census interval affected by a cyclone (see black triangles in Fig. 1b), or (2) any plot having had at least one cyclone disturbance, even minor, since 1971. The resulting datasets had respectively 23 and five plots, and 69 and 15 species presenting over 400 observations. We generated the latent survival probabilities per stem per year (*K_lat*) for each species separately, on the basis of these two datasets (see eqs. 1), and ran models M3 and M4 to test for plot-level and species-level temporal trends in mortality risk. All four resulting sensitivity analyses indicated the mortality risk trend remained clear across plots and species, even after removing the main impact of major wind-related disturbances (Fig. S4, Table S6).

Modelling climate over time: To explore the implications of the differences in mortality risk with long-term mean climate and species' position on their climatic niche, we built a separate set of models to investigate temporal trends in Tmax, VPD, and MCWD from 1971 to 2019. To do so, we used Bayesian generalised additive models, modeled the monthly values of the three climate variables separately with B-splines and a maximum of four basis functions to constrain the wiggliness of the relation [81], and added varying intercepts for the different plots. The resulting trends indicated a strong increase of Tmax and VPD over time across all plots (consistent with results from Bauman et al. [23]), but no directional increase in MCWD (Fig. 1c, Fig. S11).

Bayesian updating of the parameters: The parameter probability posteriors of the size-dependent survival models were fitted separately for each species in Stan, using the No-U-Turn-Sampler (NUTS; 5000 iterations on three chains), with the *'rstan'* R package [82]. For the models M1 and M3 to M6, Bayesian updating of the parameter probability distributions were fitted with the NUTS in Stan, by running 6000 iterations on four chains, with 1000 'warmup' steps, using the

R package *'brms'* [83] (R code in Supplementary Methods S2). Chain convergence was checked through Rhat values, ensuring they all were within 0.01 from 1, and mixing of all chains was assessed visually. Coefficient posteriors were summarised through their median and 95%-highest posterior density interval (HPDI) (i.e. the narrowest posterior interval encompassing 95% of the probability mass, corresponding to the coefficient values most consistent with the data; [81]). Model covariates were considered important when their coefficient 95%-HPDI did not encompass zero, indicating a strong-enough level of confidence to report the effect as positive or negative. All analyses were carried out in the R statistical environment [84] with R code available in Supp. Methods S2.

Data availability statement: The raw demographic data that supported the findings are available in Bradford et al. (2014; see References), in CSIRO Data Access Portal [https://doi.org/10.4225/08/59475c67be7a4], and the survival dataset used for the 81 studied species was archived on the platform of the Terrestrial Ecosystem Research Network (TERN) infrastructure [https://doi.org/10.25901/rxtc-th28], which is enabled by the Australian Government's National Collaborative Research Infrastructure Strategy (NCRIS). The climate data used in the models are openly available under the same DOI, and trait data will be made available upon reasonable request.

Code availability statement: A detailed and commented R code supporting the findings is in Supplementary Methods S2 as well as on the same TERN repository as the data [https://doi.org/10.25901/rxtc-th28].

Methods references

57. Bradford, M. G., Murphy, H. T., Ford, A. J., Hogan, D. L. & Metcalfe, D. J. Long-term stem inventory data from tropical rain forest plots in Australia. *Ecology* **95**, 2362–2000 (2014).
58. Johnson, D. J. *et al.* Climate sensitive size-dependent survival in tropical trees. *Nat. Ecol. Evol.* **2**, 1436–1442 (2018).
59. Needham, J., Merow, C., Chang-Yang, C.-H., Caswell, H. & McMahon, S. M. Inferring forest fate from demographic data: from vital rates to population dynamic models. *Proc. Biol. Sci.* **285**, 20172050 (2018).

60. Lewis, S. L. *et al.* Tropical forest tree mortality, recruitment and turnover rates: calculation, interpretation and comparison when census intervals vary. *J. Ecol.* **92**, 929–944 (2004).
61. Reeves, J., Chen, J., Wang, X. L., Lund, R. & Lu, Q. Q. A Review and Comparison of Changepoint Detection Techniques for Climate Data. *J. Appl. Meteorol. Climatol*. **46**, 900–915 (2007).
62. Clark, J. S., Bell, D. M., Kwit, M. C. & Zhu, K. Competition-interaction landscapes for the joint response of forests to climate change. *Glob. Chang. Biol.* **20**, 1979–1991 (2014).
63. Oliva, J., Stenlid, J. & Martínez-Vilalta, J. The effect of fungal pathogens on the water and carbon economy of trees: implications for drought-induced mortality. *New Phytol.* **203**, 1028–1035 (2014).
64. Franklin, J. F., Shugart, H. H. & Harmon, M. E. Tree Death as an Ecological Process. *BioScience* **37**, 550–556 (1987).
65. Yanoviak, S. P. *et al.* Lightning is a major cause of large tree mortality in a lowland neotropical forest. *New Phytol*. **225**, 1936–1944 (2020).
66. Preisler, Y., Tatarinov, F., Grünzweig, J. M. & Yakir, D. Seeking the 'point of no return' in the sequence of events leading to mortality of mature trees. *Plant Cell Environ.* **44**, 1315–1328 (2020).
67. Aragão, L. E. O. C. *et al.* Spatial patterns and fire response of recent Amazonian droughts. *Geophys. Res. Lett.* **34**, L07701 (2007).
68. Malhi, Y. *et al.* The linkages between photosynthesis, productivity, growth and biomass in lowland Amazonian forests. *Glob. Chang. Biol.* **21**, 2283–2295 (2015).
69. Hutchinson, M. F., Kesteven, J. L. & Xu, T. Making the most of the ground based meteorological network using anomaly-based interpolation. *Proceedings Session 5 of The Australian Energy and Water Exchange Initiative OzEWEX 2014* (2014).
70. Abatzoglou, J. T., Dobrowski, S. Z., Parks, S. A. & Hegewisch, K. C. TerraClimate, a high-resolution global dataset of monthly climate and climatic water balance from 1958-2015. *Sci*

Data **5**, 170191 (2018).

71. Carscadden, K. A. *et al.* Niche Breadth: Causes and Consequences for Ecology, Evolution, and Conservation. *Q. Rev. Biol.* **95**, 179–214 (2020).
72. Swenson, N. G. *et al.* A Reframing of Trait–Demographic Rate Analyses for Ecology and Evolutionary Biology. *Int. J. Plant Sci.* **181**, 33–43 (2020).
73. Morueta-Holme, N. *et al.* Habitat area and climate stability determine geographical variation in plant species range sizes. *Ecol. Lett.* **16**, 1446–1454 (2013).
74. Brum, M. *et al.* Hydrological niche segregation defines forest structure and drought tolerance strategies in a seasonal Amazon forest. *J. Ecol.* **107**, 318–333 (2019).
75. Chitra-Tarak, R. *et al.* The roots of the drought: Hydrology and water uptake strategies mediate forest-wide demographic response to precipitation. *J. Ecol.* **106**, 1495–1507 (2018).
76. Boria, R. A., Olson, L. E., Goodman, S. M. & Anderson, R. P. Spatial filtering to reduce sampling bias can improve the performance of ecological niche models. *Ecol. Modell.* **275**, 73–77 (2014).
77. Farquhar, G. D., von Caemmerer, S. & Berry, J. A. A biochemical model of photosynthetic CO2 assimilation in leaves of C3 species. *Planta* **149**, 78–90 (1980).
78. Duursma, R. A. Plantecophys--An R Package for Analysing and Modelling Leaf Gas Exchange Data. *PLoS One* **10**, e0143346 (2015).
79. De Kauwe, M. G. *et al.* A test of the 'one-point method' for estimating maximum carboxylation capacity from field-measured, light-saturated photosynthesis. *New Phytol.* **210**, 1130–1144 (2016).
80. Bloomfield, K. J. *et al.* The validity of optimal leaf traits modelled on environmental conditions. *New Phytol.* **221**, 1409–1423 (2019).
81. McElreath, R. *Statistical Rethinking: A Bayesian Course with Examples in R and STAN*. (CRC Press, 2020).

82. Stan Development Team. “RStan: the R interface to Stan.” R package version 2.21.2, http://mc-stan.org/. (2020).

83. Bürkner, P.-C. brms: An R Package for Bayesian Multilevel Models Using Stan. *J. Stat. Softw.* **80**, 1–28 (2017).

84. R Core Team. R: A language and environment for statistical computing. R Foundation for Statistical Computing, Vienna, Austria. URL https://www.R-project.org/. (2021).

85. Dinerstein, E. *et al.* An Ecoregion-Based Approach to Protecting Half the Terrestrial Realm. *Bioscience* **67**, 534–545 (2017).

Acknowledgments

We thank Alex Cheesman for his help with field work in Bellenden Ker, and Mireia Torrello Raventos for the first census of Bellender Ker. DB was funded by the Belgian American Educational Foundation (BAEF), the Philippe Wiener - Maurice Anspach Foundation, and the European Union's Horizon 2020 research and innovation programme under the Marie Skłodowska-Curie grant agreement No. 895799. GD was supported by the Philippe Wiener - Maurice Anspach Foundation. YM was supported by the Frank Jackson Foundation. JAG was funded by the UK Natural Environmental Research Council (NERC; grants NE/T011084/1 and NE/S011811/1). The trait campaign and data analysis were funded by NERC Grant NE/P001092/1 to YM and European Research Council projects T-FORCES (Tropical Forests in the Changing Earth System; 291585) to OLP and YM, and GEM-TRAIT (321131) to YM, under the European Union's Seventh Framework Programme (FP7/2007-2013). We acknowledge the foresight of Dr. Geoff Stocker in establishing the CSIRO permanent plots and the many CSIRO staff and volunteers who have helped to measure and maintain the plots since 1971. We are thankful to the Daintree Rainforest Observatory for providing a subsidy on accommodation and station fees, and thank the Australian Supersite Network, part of the Australian Government's Terrestrial Ecosystem Network (Daintree Rainforest, Cow Bay, and Robson Creek Supersites) for provision of data used as part of the study. Computational resources have been provided by the Consortium des Équipements de Calcul Intensif (CÉCI), funded by the Fonds de la Recherche Scientifique de Belgique (F.R.S.- FNRS) under Grant No. 2.5020.11 and by the Walloon Region. This study is a product of the Global Ecosystems Monitoring (GEM) network.

Author contribution statement

DB and SMM designed the study and the statistical models of tree survival. DB tidied and vetted the demographic and trait data and performed the analyses. DB led the writing with regular feedback from SMM, YM, and CF on intermediate stages of the analyses and manuscript. GD extracted species biographic data and the climatology associated with their locations to calculate species climatic niches. SR helped generate the climatic covariates. LC and LPB led the trait data collection, assisted by RD, BEM, HN, JC and PS and initiated and supported by YM. MH provided the raw climate product from ANUClimate. MB supplied demographic data for the 20 CSIRO plots and Robson Creek. CF, LC, SR, JAG, GD provided feedback on the discussion. SGWL contributed demographic data of Daintree Observatory and commented on the manuscript. All authors commented on the manuscript and gave their approval for the publication.

Competing interest

The authors do not have any competing interest to declare.

Extended data legends

Fig. S1: Schematic illustration of the size-dependent multilevel survival model and its parameters. Survival probability per year (theta) for a given species is defined by either one of two similar logistic functions, depending on a DBH threshold, only changing in the sign of *r* (*r1* > 0, *r2* < 0), yielding two S-shaped logistic function related through their common plateau *K*. This size-dependent model of survivorship was fitted separately for each of the 81 studied species. *p1* and *p2* are the inflection points of the two curves, with *p2* characterising the species DBH at 50% survival per year. *r1* and *r2* are rates of survival change per year in the corresponding portions of the survival curve. While *K* was initially the background survival rate of the species during most of the tree live [58,59], our model decomposes *K* into a species-specific average survival rate per year across all the sites and years (*K_*μ), a site-specific deviation from the average (*K_P*), a year-specific deviation from the average *(K_T*), and an error term (not represented, here). Because nearly all species occurred in multiple plots, and because different plots were recensused on different years, every two to five years mostly, the overlap of census years across plots allowed us to infer a latent survival probability per year, between 1971 and 2019 (*K_lat*). *K_lat*, the latent logit-survival probability per year, generated separately for each species through this survival model, was used as the response variable of all subsequent analyses (M1 to M6, see Table S4) to study how species' mortality risk (i.e. 1 - survivorship, or 1 - *K*) changed through the years, whether this change varied among species and sites, and how climate, species' climatic niche, and species functional traits related to mortality risk changes through time. Examples of the above theoretical curve from some of the studied species are presented in Fig. S2.

Fig. S2: Illustration of the interspecific variability of survival probability as a function of tree diameter. The figures represent species-specific survival probability predictions between 10 and 160 cm DBH for four of the 80 species of the study, across forest plots and years, based on the species-specific Bayesian multilevel models of survival (eqs. 1; Fig. S1). The red line is the posterior survival probability per year median, and the dark and light grey shaded areas are the 50%- and 90% posterior credibility intervals, respectively. Vertical dashed lines correspond to the observed maximum DBH for the corresponding species (*Acacia celsa Tindale*,

Acronychia laevis J.G.Forest & G.Forst, *Cardwellia sublimis F.Muell.*, and *Flindersia bourjotiana F.Muell.*).

Fig. S3: Effects of local climate on average mortality risk and mortality risk temporal change across plots (models M3). Model M3 tests the effect of 'year', and either Tmax and MCWD, or VPD and MCWD on mortality risk (see eqs. 3; Tmax and VPD tested in separate models to limit collinearity, see Supp. Methods S1). Climate variables influence the model grand intercept (average mortality risk across plots, α_0) and grand 'year' slope (mortality risk increase over time, β_0), through coefficients $\alpha_{1\text{-}2}$ and $\beta_{1\text{-}2}$, respectively. Average mortality risk is higher in plots presenting on higher long-term mean monthly Tmax and VPD during the warmest/driest quarter (95%-HPDI of α_1 encompass positive values only). Mean climate does not clearly predict how steep the temporal increase in mortality risk is among the plots (95%-HPDI encompass zero).

Fig. S4: Sensitivity analyses of the mortality risk increase over time: Species-level and plot-level slopes of change of mortality risk per year (1984-2019) without influence of cyclones. a, c: Plot-level (a) and species-level (c) slopes of mortality risk change per year (β_k and β_j, respectively; eqs. 3 and 4), obtained with models M3 and M4 on the basis of the subset of survival data obtained from the first approach to remove the effect of cyclones: Any census interval in a plot damaged by a cyclone was removed from the initial dataset, and the Bayesian size-dependent survival model (eqs. 1) was run for the species that presented > 400 observations in the reduced dataset. Models M3 and M4 were then run on the resulting latent survival probabilities *K_lat* (see eqs. 1, 3, 4) to test for temporal changes in mortality risk across plots and species, with plot-level and species-level slopes. b, d: The second approach to remove the influence of cyclones consisted of only keeping the plots that remained totally unaffected by cyclones in the last 49 years (see Suppl. Methods S1), then selecting the species that had > 400 observations in the remaining plots, generating the latent survival probability per year (*K_lat*; eqs. 1), and running models M3 and M4 as for the first approach. a-d: Species and plots whose 95%-highest posterior density interval (HPDI) encompassed zero are half-transparent. Blue and red circles indicate clear mortality increase and decrease through time, respectively (intervals not encompassing zero). The black vertical solid and dashed lines are the median and 95%-HPDI of the grand 'year' slope (i.e. generalisable effect across plots (a, b) and species (c; d)). The two approaches to test the robustness of the mortality risk temporal change without the main influence of cyclones (removal of intervals, or removal of plots) respectively had 69 and 15 species, and 23 and five plots The percentage and number of plots and species

whose mortality risk increased between 1984 and 2019 for approach 1 and 2 respectively were 96% (22) and 100% (5) of the plots, and 81% (56) and 92% (11) of species.

Fig. S5: Illustration of functional trait relationships among the 40 species with trait data, used in the M6 models of mortality risk over time. The figures represent the functional space occupied by the 40 tree species on the first four ordination axes of a correlation PCA, together describing 71.4% of the trait values (see Table S3 for trait abbreviations).

Fig. S6: Effects of species functional traits on average mortality risk and mortality risk change through time. a,b: Trait mediation of species-level intercept and 'year' slopes (α_1 and β_1, respectively, see eqs. 6 in Suppl. Methods S1). a: Positive and negative slopes indicate traits increasing and decreasing average mortality risk, respectively. b: Positive slopes correspond to traits that accentuate the rate of mortality risk change per year, while negative slopes correspond to attenuations of this rate. Circles and intervals are median and 95%-highest posterior density intervals (HPDI) for slope coefficients α_1 (trait effect on average mortality risk) and β_1 (trait mediation of 'year' effect on mortality risk) (see eqs. 6).

Fig. S7: Change of stand-level basal area per hectare (BA) over time. Change of BA per forest plot between 1971 and 2019 (a). Each circle is a plot BA on the year beginning a census period. The smooth curve and shaded area are the mean and 95% confidence interval of a generalised additive model (GAM), showing a decrease in plot BA across plots, and within most plots. The circle colour is proportional to the BA value (yellow to blue for low to high BA).

Fig. S8: Living and dead tree DBH distributions for the time period 1984-2019. The histogram bins are 1 cm-wide. We explored the relation between increased mortality risk and tree DBH visually and did not detect any clear size association. A Pearson's Chi-squared test with simulated p-value confirmed that no clear link could be detected between the proportions of alive and dead individuals in DBH bins of 1 or 5 cm ($\text{Chi-squared}_{\text{bin\_5cm}} = 0.0054$, p-value = 1).

Fig. S9: Changes of log-transformed absolute diameter growth rate (AGR) over time across and within species, for the 81 studied species. The main figure shows the species-level coefficients of AGR change per year, between 1971 and 2019 (species-specific 'year' slope; β_{2j} in eqs. 7, Supp. Methods S1). Circles and horizontal bars are posterior median and 95% highest posterior density intervals (HPDI). Plain black circles and bars are species whose posterior 95%-HPDI did not encompass zero; semi-transparent circles and bars are species whose HPDI encompassed zero (no clear AGR increase or decrease). The red dashed line marks zero, that

is, the separation between coefficient values indicating an increase of AGR over time (positive values) and a decrease of AGR over time (negative values). The vertical plain and dashed blue lines are the median and 95%-HPDI of the grand year slope (see inset). The inset shows the posterior probability distribution of the coefficient of AGR change per year across all species (i.e. grand 'year' slope mean; $\beta_{2,0}$ in eqs. 7, Supp. Methods S1). Overall, AGR did not clearly increase or decrease across species (unlike mortality risk; Fig. 3). AGR increased for 14 species and decreased for 19 species, while remaining mostly unchanged (95%-HPDI encompassing zero) for 48 species (semi-transparent circles and horizontal bars).

Fig. S10: Comparison of the climatic space occupied by the 24 plots of Australian tropical moist forests of the study with the total climatic space of tropical moist forests worldwide. The climatic spaces were obtained from 30-year climate averages (1981-2010) extracted from TerraClimate [70], combined with the spatial locations of the grid cells belonging to the biomes "Tropical and subtropical moist broadleaf forests" (including tropical montane forests) ([85]; see https://ecoregions2017.appspot.com/).

Fig. S11: Overall temporal trends in climate across the environmental gradient. Three Bayesian B-spline models with varying plot intercept and four basis functions were used to model monthly VPD, Tmax and MCWD over time across all 24 plots (see Methods). Both temperature and VPD showed a strong increase across all plots. MCWD did not show any clear directional trend across plots (more details in Bauman et al. 2021).

Additional information statement

Supplementary Information is available for this paper. Correspondence and data request should be addressed to David Bauman. Reprints and permissions information is available at www.nature.com/reprints

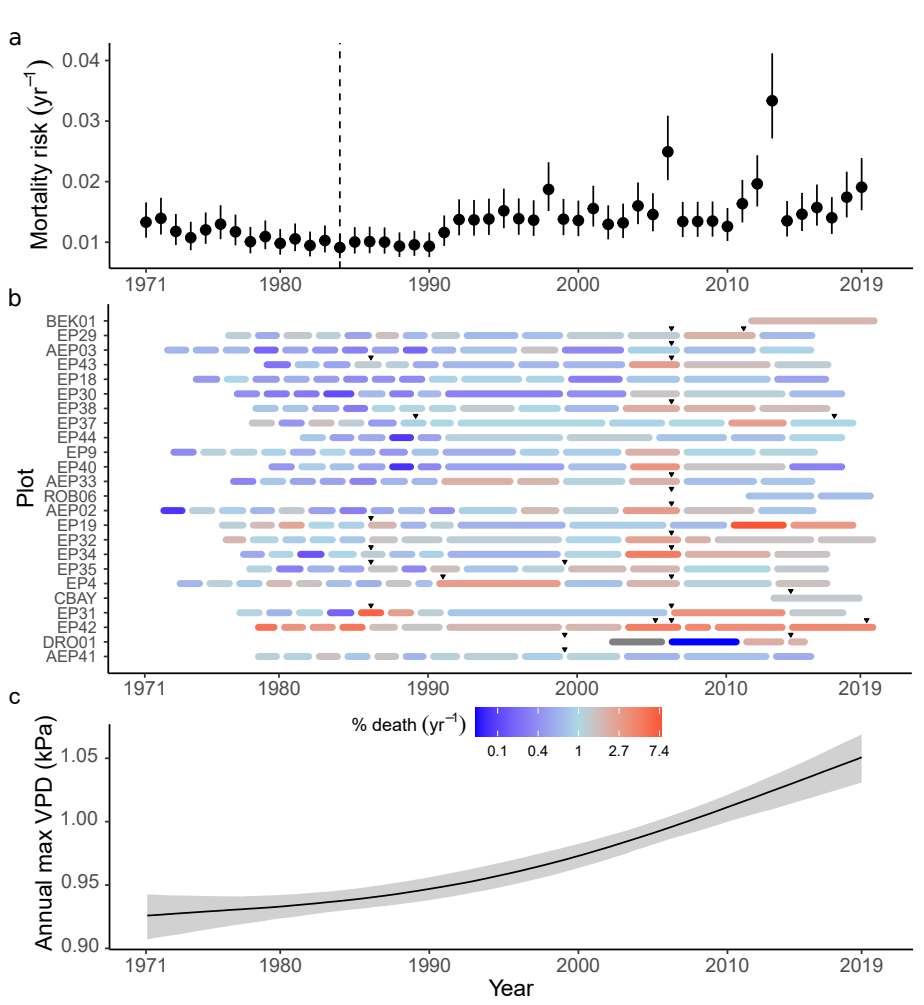
a
Mortality risk (yr^{-1})
0.04
0.03
0.02
0.01
1971
1980
1990
2000
2010
2019
b
Plot
BEK01
EP29
AEP03
EP43
EP18
EP30
EP38
EP37
EP44
EP9
EP40
AEP33
ROB06
AEP02
EP19
EP32
EP34
EP35
EP4
CBAY
EP31
EP42
DRO01
AEP41
1971
1980
1990
2000
2010
2019
c
% death (yr^{-1})
0.1
0.4
1
2.7
7.4
Annual max VPD (kPa)
1.05
1.00
0.95
0.90
1971
1980
1990
2000
2010
2019
Year

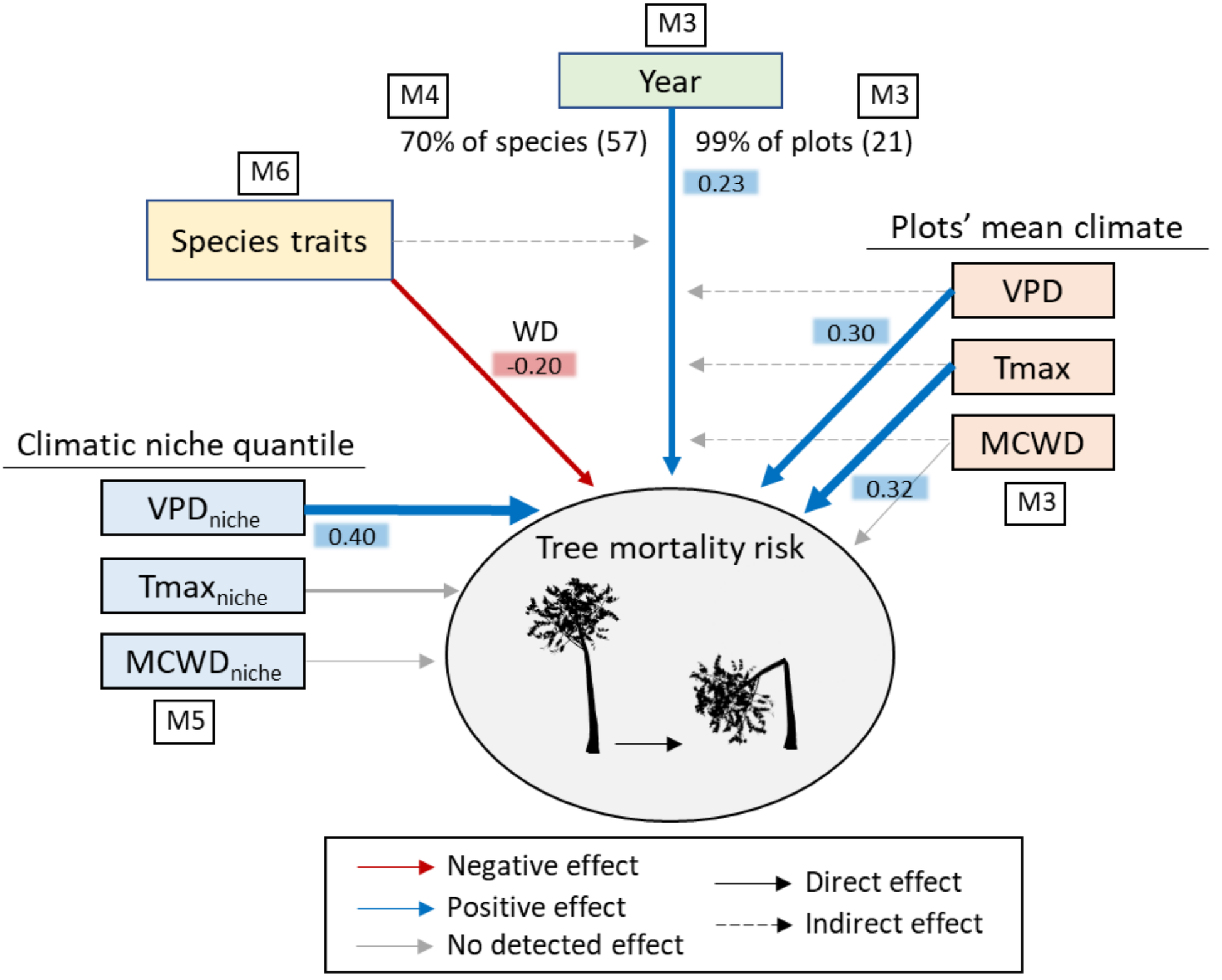

M3 → Mortality risk ~ year, with plot-level slopes depending on local climate
M4 → Mortality risk ~ year, with sp-level slopes
M5 → Mortality risk ~ year and position on climatic niche, with sp-level slopes
M6 → Mortality risk ~ year, with sp-level slopes depending on functional trait

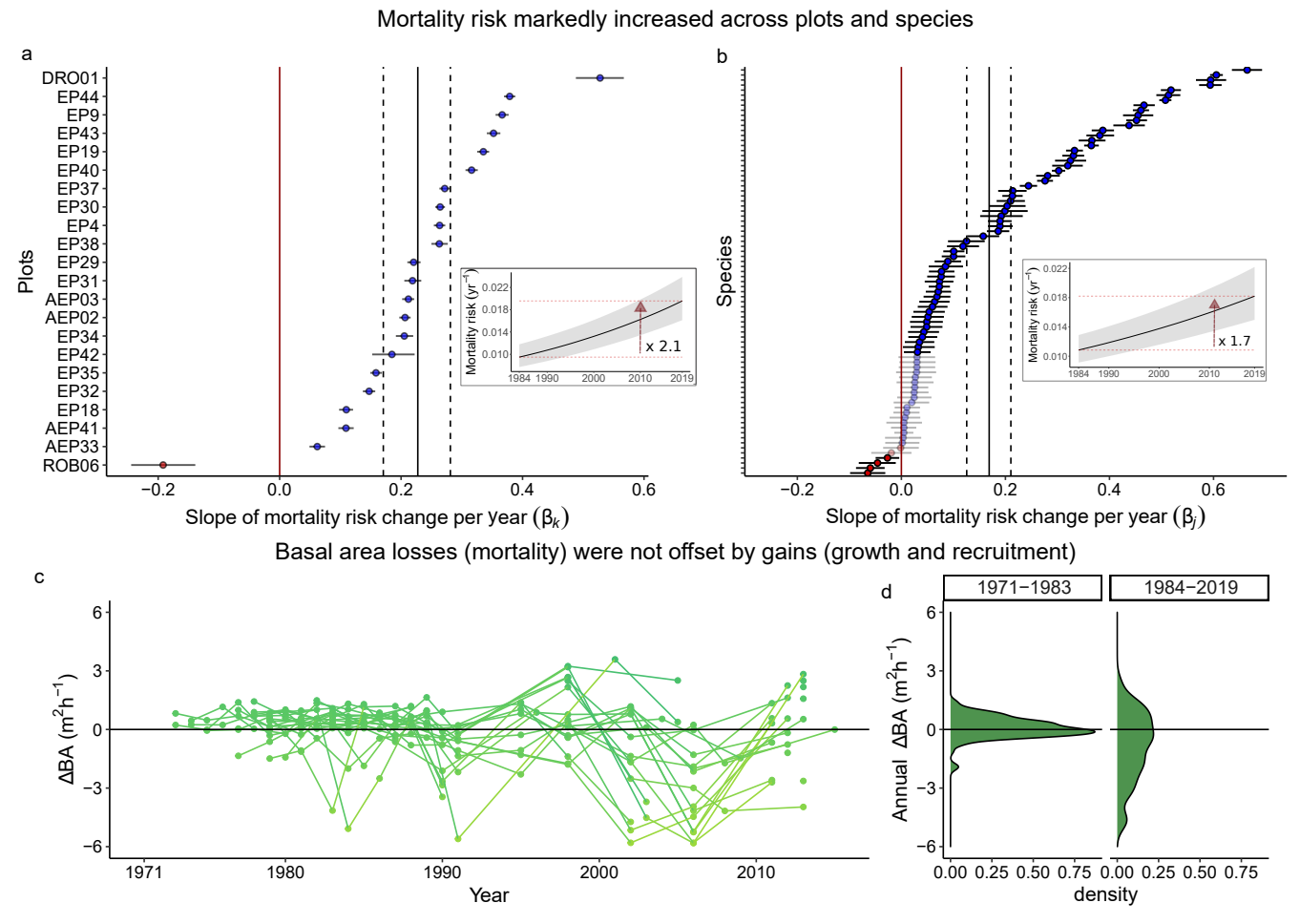
Mortality risk markedly increased across plots and species
a
b
Plots
Species
DRO01
EP44
EP9
EP43
EP19
EP40
EP37
EP30
EP4
EP38
EP29
EP31
AEP03
AEP02
EP34
EP42
EP35
EP32
EP18
AEP41
AEP33
ROB06
−0.2
0.0
0.2
0.4
0.6
Slope of mortality risk change per year (β_k)
Slope of mortality risk change per year (β_j)
Mortality risk (yr^{-1})
0.022
0.018
0.014
0.010
1984
1990
2000
2010
2019
x 2.1
x 1.7
Basal area losses (mortality) were not offset by gains (growth and recruitment)
c
d
ΔBA (m^{2}h^{-1})
6
3
0
−3
−6
1971
1980
1990
2000
2010
Year
1971−1983
1984−2019
Annual ΔBA (m^{2}h^{-1})
0.00
0.25
0.50
0.75
density

From species' biogeography and climate to species' position on their climatic niche

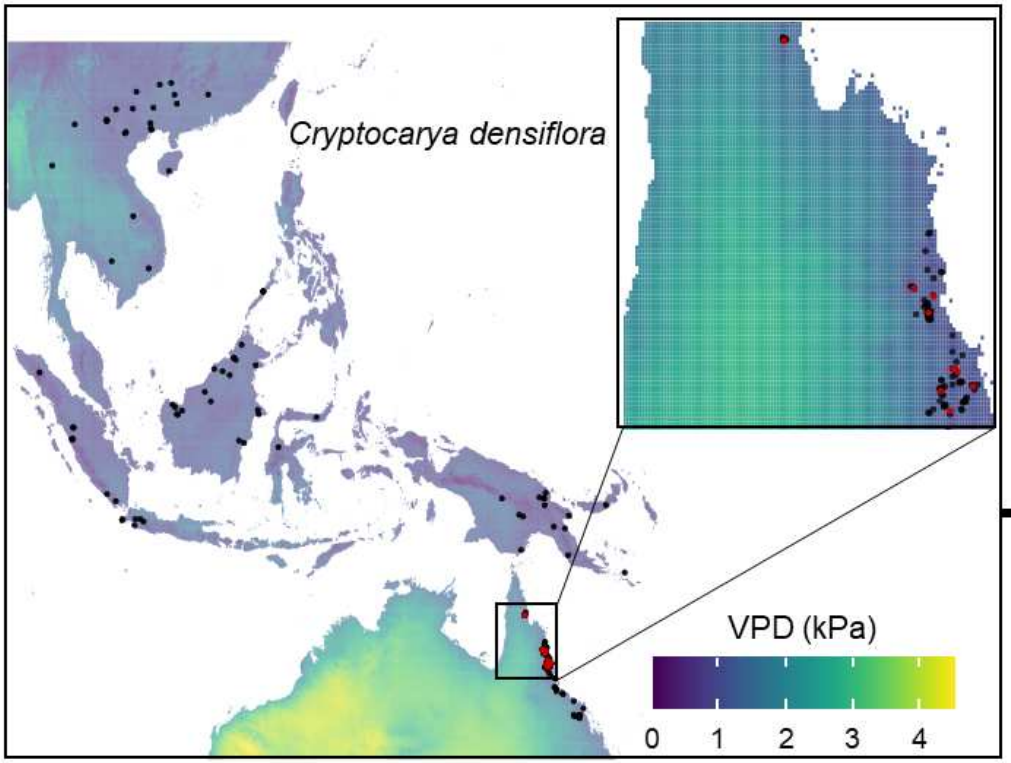

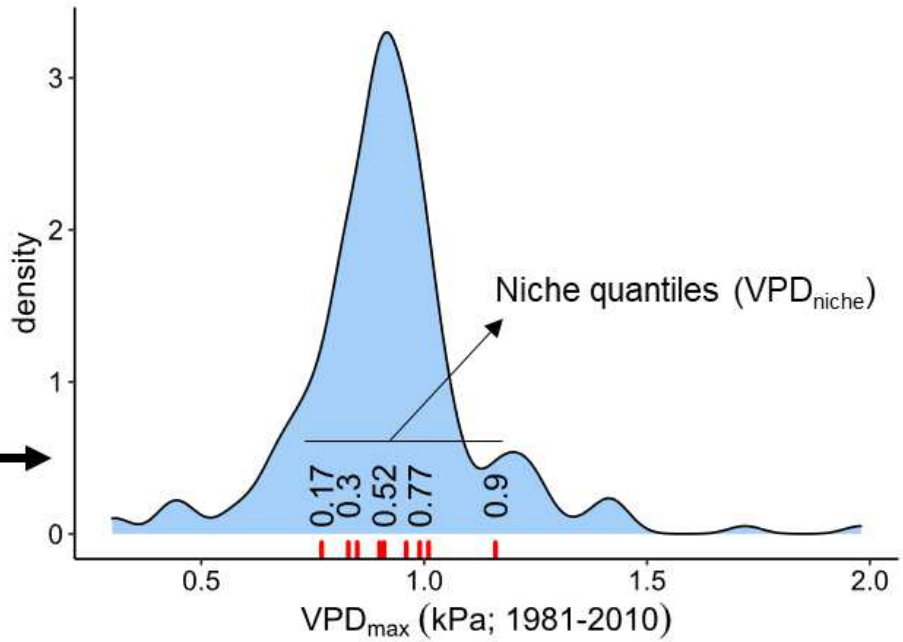

79% of species have higher average mortality risk closer to the upper edge of their VPD niche